Solar Energy Materials & Solar Cells 248 (2022) 111931

Contents lists available at ScienceDirect

Solar Energy Materials and Solar Cells

journal homepage: www.elsevier.com/locate/solmat

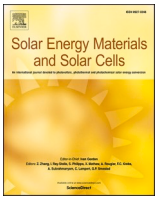

Contactless measurement of current-voltage characteristics for silicon solar cells

Johannes M. Greulich [a,*], Wiebke Wirtz [a,b], Hannes Höffler [a], Nico Wöhrle [a], Mattias K. Juhl [c], Oliver Kunz [c], Stefan Rein [a], Andreas W. Bett [a,d]

[a] Fraunhofer Institute for Solar Energy Systems (ISE), Heidenhofstraße 2, 79110, Freiburg, Germany
[b] Now with Institute for Solar Energy Research Hamelin, Am Ohrberg 1, 31860, Emmerthal, Germany
[c] University of New South Wales, School of Photovoltaics and Renewable Energy Engineering, Tyree (H6), University Mall, Kensington NSW, 2052, Australia
[d] University of Freiburg, Institute of Physics, Hermann-Herder-Straße 3, 79104, Freiburg, Germany

ARTICLE INFO

Keywords:
Silicon solar cell
Current-voltage characteristics
Contactless
Non-contact
Optics

ABSTRACT

The measurement of the current-voltage (*IV*) characteristics is the most important step for quality control and optimization of the fabrication process in research and industrial production of crystalline silicon solar cells. We propose a methodology to determine the *IV* characteristics of silicon solar cells in a contactless way. We summarize the theory behind the method, describe the experimental setup and prove the validity of the concept by comparing contactless with conventionally measured *IV* results. We demonstrate that the differences in open-circuit voltage, short-circuit current, fill factor, and efficiency are smaller than 2.5 $\%_{rel}$ for a test set consisting of four passivated emitter and rear cells (PERC cells), two tunnel oxide passivated contact (TOPCon) cells and a silicon heterojunction (SHJ) cell. The methodology eliminates mechanical stress on the solar cells and the time required for contacting the cells, does not require broad busbars for contacting and, hence, enables to reduce the silver consumption, simplifies the measurements of shingle cells and potentially shortens the required time, avoids shading by the contact units and consumable costs for the probes, and yields additional information (reflectance spectrum, quantum efficiency) on the cells compared to conventional *IV* testing. The methodology might facilitate further applications in the future, e.g., contactless outdoor testing of modules, individual diagnosis of failed cells within a module, and on-the-fly *IV* measurements of cells.

1. Introduction

Conventional *IV* measurements for solar cells in mass production are based on a stop-and-go routine with a solar simulator providing uniform and well-defined illumination, and probe bars contacting the cell on front and rear side whilst current *I* and voltage *V* are measured in a four-wire setup to eliminate measurement artifacts resulting from series resistance in the wires and the probes. Today, typically 4 to 12 probe bars per cell side are used in mass production, depending on the number of busbars on the cell. This procedure has several disadvantages: First, the contacting induces mechanical stress into the cells and might lead to cell breakage. Second, the time required for decelerating the cell, moving the contact bars down and up and then accelerating the cell again requires 72% or more of the cycle time [1] and might become a limiting factor in throughput if it is not already at present. The throughput is also compromised by longer measurement times that are indicated for the *IV* measurements to reduce hysteresis effects (see e.g. Refs. [2,3]). Furthermore, the probe bars shade the underlying cell and, hence, in fact cause a much more inhomogeneous illumination than without the probe bars. Next, rather broad busbars are required for conventional contacting units based on spring-loaded pins and, hence, silver consumption is enhanced. Finally, the spring-loaded pins of the probe bars or the probe bars themselves are consumable material and must be replaced after a certain amount of contacting events, which constitutes non-negligible maintenance costs and downtime. For individual shingle cells, the contacting is much more complicated than for conventional cells [4] and the throughput in W_p/h is significantly reduced. These issues can be alleviated or completely avoided by implementing an approach totally avoiding a contacting of the cells. Such a contactless *IV* measurement approach is demonstrated in the present work.

The contactless measurement of the Suns-photoluminescence (Suns-

* Corresponding author.
E-mail address: johannes.greulich@ise.fraunhofer.de (J.M. Greulich).

https://doi.org/10.1016/j.solmat.2022.111931
Received 29 April 2022; Received in revised form 25 July 2022; Accepted 27 July 2022
Available online 6 September 2022

PL) pseudo-*IV* characteristics, equivalent to Suns-open-circuit voltage (V_{oc}) characteristics of solar cells have been introduced by Trupke et al. [5] via measurement of photoluminescence (PL) and incident light intensity. The spectral hemispherical reflectance $R(\lambda)$ can already be measured in a contactless way and fast enough for inline application, e. g. using white light illumination, an integrating sphere and a spectrophotometer [6]. Contactless electroluminescence (EL) for silicon solar cells was introduced by Sinton et al. [7] to determine the shunt or parallel resistance of solar cells. The technique is based on illuminating a first part of the free-standing device under test and detecting luminescence radiation emitted in a second, shaded part of the device. It avoids the detection of luminescence signal originating from diffusion-limited charge carriers [8]. A contactless technique to determine the relative quantum efficiency of cell precursors based on photoconductance measurements was proposed by Mäckel et al. [9]. For precursors and cells including metallization, a similar approach based on photoluminescence was proposed [10,11]. In these techniques, diffusion-limited charge carriers generate artifacts in particular in exceedingly high quantum efficiencies between 800 and 1200 nm [12]. Diffusion-limited charge carriers are generated by absorption of light, and their collection at the p-n junction is limited by a finite diffusion length. Their concentration is independent of the applied voltage, they do not contribute to the external current, but influence measurements of the photoconductivity and implied voltage. To avoid these artifacts, the contactless EL approach was successfully applied [13] and optimized [14,15]. Additionally, the luminescence spectrum $\varphi_{\mathrm{Lum}}(\lambda)$ emitted by the cell at 1000 nm–1200 nm can be analyzed, from which the relative external quantum efficiency can be calculated using Rau's spectral reciprocity theorem [16,17]. For a contactless, yet qualitative determination of the series resistance r_s, Kasemann et al. proposed to generate internal currents via partial shading of the cells and detect the luminescence images under partial shading conditions, in addition to a PL image under homogeneous illumination [18]. A similar approach based on a projection of a light pattern via a digital micromirror device was presented by Zhu et al. [19]. Zafirovska et al. have shown that even with a line scan camera and a line-shaped illumination, series resistance contrasts are qualitatively visible in luminescence images [20]. In contrast to these qualitative approaches based on homogeneously and partially illuminated luminescence, Höffler et al. presented very recently an approach to analyse such data for a quantitative and contactless determination of the series resistance [21].

With the present work, we combine some of the known methods, improve on the existing approaches by scaling the relative quantum efficiency to absolute quantum efficiency and exploit the enabling feature of Höffler's work that the r_s can be detected quantitatively.

2. Theory

The approach for the contactless determination of the current-voltage characteristics under forward bias is based on four pillars: (i) Suns-photoluminescence (Suns-PL, [5]) to obtain V_{oc} and the pseudo-*IV*-characteristics including pseudo fill factor pFF, (ii) spectral reflectance measurements and (ii) contactless measurements of the external quantum efficiency EQE [13,14] to determine j_{sc}, and (iv) contactless measurements of the cell's series resistance r_s [21] to calculate the fill factor FF and the energy conversion efficiency.

Suns-PL measures the PL intensity φ as a function of incident photon flux *N,* and can provide data equivalent to the Suns-V_{oc} characteristics [5]. The PL intensity φ is calibrated to voltage V with a calibration constant C via

$$V\left(N\right) = V_t \cdot \ln\left(\frac{\varphi(N)}{C}\right) = V_t \cdot \ln(\varphi(N)) - V_t \cdot \ln\left(C\right) \tag{1}$$

with the thermal voltage $V_t = kT/q$ (about 26 mV at room temperature). The calibration constant can be determined based on the PL intensity and known V_{oc} of a calibrated reference cell.

The spectral hemispherical reflectance $R(\lambda)$ can already be measured in a contactless way and fast enough for inline application. For that purpose, diffuse white light illumination of the cell is recommended. The reflected light is detected at an angle almost perpendicular to the sample surface using a multichannel spectrophotometer [6]. The calibration of the intensity signal is done using a light trap as black standard and a white standard.

We apply electroluminescence excitation spectroscopy (ELE, [13,14]) to determine the relative external quantum efficiency

$$EQE_{\mathrm{ELE}}(\lambda) = \frac{\varphi_{\mathrm{ELE}}}{N(\lambda)} \tag{2}$$

with the integral luminescence intensity φ_{ELE} and the incident photon flux N at the wavelength λ. The luminescence signal is detected in a shaded part of the cell while the rest of the cell is illuminated, thus avoiding diffusion-limited charge carriers to contribute to φ_{ELE}.

In the near-bandgap region of the spectrum, applying ELE might present two problems: First, it is more complicated assigning a specific wavelength to the measured signal when using LED illumination with a non-monochromatic spectrum since the EQE is typically a steep and convex curve there [15]. Second, potential stray light of the excitation light source entering the detector must be suppressed by several orders of magnitude only with mechanical separation - optical dielectric or absorptive filters in front of the detector apply to both, excitation light and luminescence radiation, equally since both lie in the same spectral region. To alleviate or even overcome these obstacles, the ELE data can be combined with a measurement of the luminescence spectrum to determine the EQE based on the reciprocity theorem [16,17], $EQE_{\mathrm{rt}}(\lambda)$. By claiming a steady continuation of EQE_{ELE} and EQE_{rt} at ~1000 nm, i.e. $EQE_{\mathrm{ELE}}(\lambda = 1000\ \mathrm{nm}) = EQE_{\mathrm{rt}}(\lambda = 1000\ \mathrm{nm})$, they can be joined to yield the relative EQE_{rel}. Now, we propose to calculate the internal quantum efficiency as

$$IQE_{\mathrm{contactless}}(\lambda) = S \cdot \frac{EQE_{\mathrm{rel}}(\lambda)}{1 - R(\lambda)}. \tag{3}$$

We suggest to determine the scaling factor S for each cell individually by setting $IQE_{\mathrm{contactless}}(\lambda = \lambda_{\mathrm{cal}}) = 100\%$ [22,23]. Here, we use $\lambda_{\mathrm{cal}} \approx 660$ nm for front junction silicon solar cells. In this wavelength range, the light is absorbed in silicon close to the p-n junction within the base without major collection losses neither from the emitter nor from the base. For back-junction cells, we scale the maximum of $IQE_{\mathrm{contactless}}$ to 100%, no matter at which wavelength the maximum occurs for lack of a better alternative. The short-circuit current density j_{sc} can then be determined as

$$j_{sc} = \int q \cdot EQE(\lambda) \cdot \varphi_{\mathrm{AM1.5g}}(\lambda) \cdot \mathrm{d}\lambda \tag{4}$$

based on the photon flux $\varphi_{\mathrm{AM1.5g}}(\lambda)$ of the AM1.5g spectrum at 1000 W/m^2 and the scaled absolute EQE spectrum $EQE(\lambda) = S \cdot EQE_{\mathrm{rel}}(\lambda)$. If required, the individual measurement points of the EQE can be interpolated based on the reflectance and analytical models for the *IQE* [24–26].

We apply a recently proposed method for measuring r_s [13]. This method is based on comparing homogeneously illuminated and partially shaded luminescence measurements. We follow Höffler's recommendation [13] to have a constant luminescence signal φ in the homogeneously and partially shaded measurements. For general illumination intensities and corresponding generated current densities $j_{\mathrm{gen,l}}$ and $j_{\mathrm{gen,hom}}$, luminescence signal intensities φ_{l} and φ_{hom} and shading fraction f, we propose the following formula for r_s

$$r_s = V_t \ln\left(\left[\frac{j_{\mathrm{gen,l}}}{j_{\mathrm{gen,hom}}} \cdot \frac{\varphi_{\mathrm{hom}}}{\varphi_{\mathrm{l}}} - 1\right] \cdot \frac{f}{1-f}\right) \cdot \frac{1-f}{j_{\mathrm{gen,hom}} \cdot \frac{\varphi_{\mathrm{l}}}{\varphi_{\mathrm{hom}}} - j_{\mathrm{gen,l}}}, \tag{5}$$

where the index "l" indicates data of the lit regions under partial shading

conditions and the index "hom" indicates data under homogenous illumination. The generated current densities can be determined from a measurement of the excitation light intensity and the EQE of the device under test. This expression generalises the formulae given by Höffler et al. for the two special cases of constant luminescence signal and constant illumination intensity [13]. Following this approach further, expressions for the series resistance based on the luminescence intensity in the shaded part combined either with homogeneously illuminated luminescence measurements or the luminescence intensity in the illuminated part under partial shading conditions can be derived, but will not be discussed here further.

The Suns-PL, j_{sc} and r_s data are converted to actual *IV* or *j(V)* characteristics via

$$j(N) = j_{sc} \cdot \left(N \,/\, N_{AM1.5g} - 1\right) \tag{6}$$

and

$$V(N) = V_t \cdot \ln\left(\frac{\varphi(N)}{C}\right) + r_s \cdot j(N), \tag{7}$$

remembering that N is the incident photon flux varied during the Suns-PL measurement. From the $j(V)$ curve, other *IV* parameters, such as the efficiency η and fill factor FF can be derived.

3. Experimental

The method is applied to four M2-sized (156.75 mm) p-type Cz-Si:B PERC (5 tapered busbars, each on average 270 µm thin), two n-type TOPCon (0 busbars) and an n-type SHJ cell (5 busbars, each 800 µm broad).

Conventional EQE and reflectance spectra are measured in a LOANA system from PVtools GmbH, Germany, on a 20 mm × 20 mm off-center spot on the cells between the busbars. Conventional illuminated *IV* and Suns-V_{oc} characteristics are measured with a AAA inline flash tester from h.a.l.m. elektronik GmbH, Germany, with a conventional contacting unit consisting of 5 bars per side equipped with spring-loaded pins for the PERC and SHJ cells and with a PCBtouch contacting unit from Pasan SA [27] for the busbarless TOPCon cells. The series resistance is determined from the maximum power point of the illuminated *IV* characteristics combined with the Suns-V_{oc} characteristics.

The spectral reflectance is measured contactless with a Zeiss MCS 700 spectrometer with an integrating sphere (OFR 104 Flare), integrated into an automated cell tester. The tool is configured to measure three spectra on a ~15 mm broad stripe in the cell's center over its full length. Each spectrum is measured within 40 ms. The contactless ELE measurements are performed with LED illumination at 11 wavelengths between 373 nm and 1175 nm (photon-flux-weighted mean wavelengths) with an intensity comparable to ~0.015 suns using a Sinus 220 solar simulator from Wavelabs Solar Metrology Systems GmbH, Germany. The luminescence intensity was measured using an InGaAs photodiode from the PL system "Modulum" [28]. Additionally, $\varphi_{Lum}(\lambda)$ is measured with a calibrated fibre-coupled InGaAs spectrometer between the wavelengths of 960 nm and 1200 nm using a contactless electroluminescence technique. This was achieved by full-area illumination of the sample, except for a shaded region of approximately 25 mm × 25 mm, from which luminescence was collected with a 400 µm multimode fibre. The contactless measurement of r_s is based on a photoluminescence (PL) imaging setup [28] incorporating a camera with a cooled Si detector, an 808 nm laser for irradiation and a shadow mask. The five busbars divide the cell into six segments 1–6. The shadow mask is shading every second segment. Two PL images are recorded under partial shading conditions, the first with segments 1, 3 and 5 shaded, the second with segments 2, 4 and 6 shaded. The same mask is also applied for the busbarless cells. The light intensity during homogeneous illumination is comparable to 1 sun ($2.5 \bullet 10^{17}$ photons/cm^2/s), while the intensity for 50% shading is set to ~1.4 suns. These intensities are chosen to roughly generate a constant signal in the non-shaded areas as detected by the camera. The Suns-PL measurements are performed with the same setup as the r_s measurements with a variation in homogeneous incident light intensity between 1 sun and ~0.005 suns. The laser intensity is measured using a calibrated Si photodiode.

4. Results and discussion

4.1. Suns-PL and Suns-V_{oc}

The comparison of V_{oc} and pFF measured in the conventional and in the contactless way is shown in Fig. 1. We observe a clear correlation of the data. The mean absolute deviation for V_{oc} is 2.1 mV and for pFF 0.39%$_{abs}$. We judge these deviations to be close to minimum since a temperature variation of 1 K induces typically a V_{oc} variation of 2 mV.

The calibration of the PL signal for each cell individually at 0.2 suns to the corresponding value of the Suns-V_{oc} curve from the contacted measurement yields calibration constants between $2.294 \bullet 10^{-8}$ and $2.418 \bullet 10^{-8}$ counts/s for the present setup. According to Eqn. (1), this corresponds to voltage differences $\Delta V = V_t \cdot \ln(C_{max}) - V_t \cdot \ln(C_{min})$ of not more than 1.35 mV. This means that the choice of the calibration constant induces a minor error of ±0.68 mV to the voltage measurement and of only ±0.01%$_{abs}$ on the pFF measurement. We conclude that it is sufficient to determine C once on a reference cell that is best chosen to be similar to the test cells.

In order to assess the potential measurement speed, we measure the

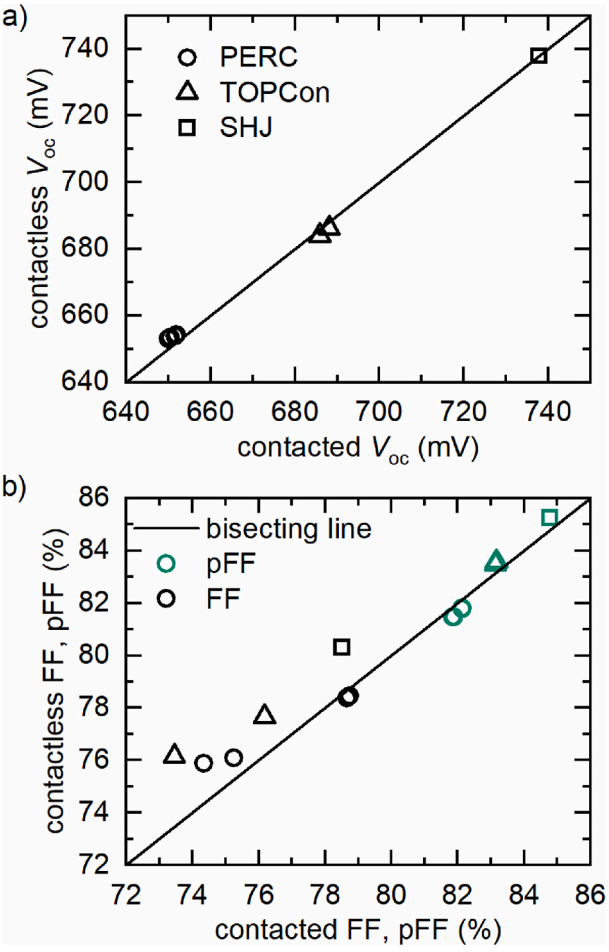

Fig. 1. The comparison of the *IV* parameters a) open-circuit voltage at 1 sun and b) actual and pseudo fill factor of the test set consisting of PERC, TOPCon and SHJ solar cells measured in a contactless and a conventionally contacted way show a clear correlation.

PL signal additionally with a PL sensor based on a InGaAs photodiode [28] for a PERC cell with V_{oc}(1sun) = 662 mV. The whole Suns-PL characteristic is measured 3 times, within 1000 ms, 500 ms, and 50 ms, respectively, each once with increasing and once with decreasing light intensity. 1000 data points are measured for each Suns-PL characteristic. V_{oc}(1sun) varies by less than 0.6 mV, pFF by less than 0.07%$_{abs}$. We judge these variations to be close to minimal, again having in mind that a temperature variation or offset during the temperature measurement of 1 K induces a V_{oc} variation of ~2 mV, both in the contacted and the contactless measurement.

4.2. Short-circuit current density

The spectral hemispherical reflectance R as measured with the Zeiss inline system and with the LOANA offline system as shown in Fig. 2 exhibit a close match. It is evident that the inline system has a more limited spectral range. For the present analysis, the values at 360 nm and 1140 nm were assumed to be valid also below 360 nm and above 1140 nm, respectively. This is a crude approximation, and the robustness of the approach can be improved with an extended spectral measurement range in the future. The slight reflectance deviations apparent in Fig. 2b for the SHJ cell might stem from lateral inhomogeneity of the sample, particularly of the transparent conductive oxide and from the broad busbars included in the inline measurement but excluded in the offline measurement.

Furthermore, Fig. 2 shows the external and internal quantum efficiency (EQE, IQE) before and after scaling as measured with the ELE technique, and the EQE as determined from the luminescence spectrum based on the reciprocity theorem. A close match with the conventionally measured EQE with contacting of the cells can be observed. We speculate that the small deviation of the EQE between 1000 nm and 1100 nm might originate from the curvature of the EQE, the finite spectral bandwidth of the spectrometer, and the non-zero width of the LED spectra and might be reduced in the future by an advanced correction procedure [15]. We further speculate that this deviation might stem from injection-dependent bulk lifetime, i.e., bias light, which is not applied for the contactless EQE measurement, while 0.3 suns bias light is applied for the contacted EQE measurements.

The noise of the EL spectrum visible in the quantum efficiency between 960 nm and 1030 nm appears to be large. It can potentially be reduced by combining the InGaAs sensor with a (cooled) Si sensor, which is expected to give a superior signal-to-noise ratio in EQE and, hence, j_{sc}.

From the contactless EQE data, the short-circuit current density j_{sc} is calculated according to Eqn. (4). As shown in Fig. 3, a good correlation with the conventionally measured, i.e. contacted, data can be observed for the test set. A mean absolute deviation of 0.32 mA/cm^2 is achieved. Whereas we observe a close match for the PERC and TOPCon cells, the j_{sc} of the SHJ cell deviates significantly more. A more detailed analysis shows that the assumption $IQE_{ELE}(\lambda_{cal}) = 100\%$ is inaccurate: the contacted IQE of the SHJ back-junction cell does not reach 100% at its maximum as assumed for the contactless evaluation but is in fact limited to 97.6%. We speculate that the remaining 2.4% loss in IQE stems from either absorptive thin films at the cell's front and/or from enhanced front surface or bulk recombination [29]. This limited IQE explains also quantitatively most of the observed j_{sc} deviation of 2.7% for the SHJ cell.

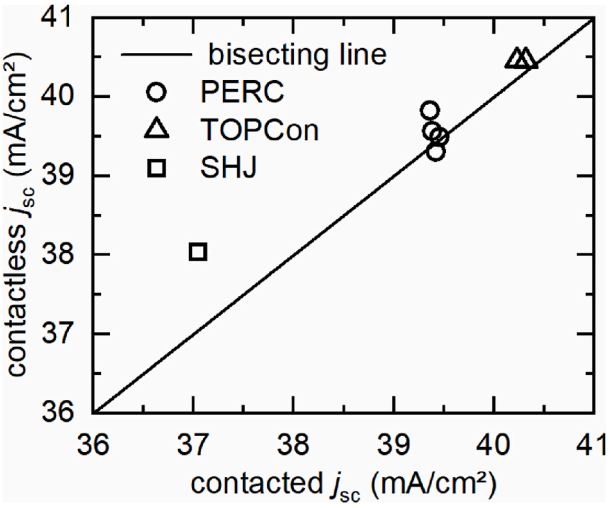

Fig. 3. The comparison of the short-circuit current density of the test set consisting of PERC, TOPCon and SHJ solar cells measured in a contactless and a conventional contacted way show a clear correlation.

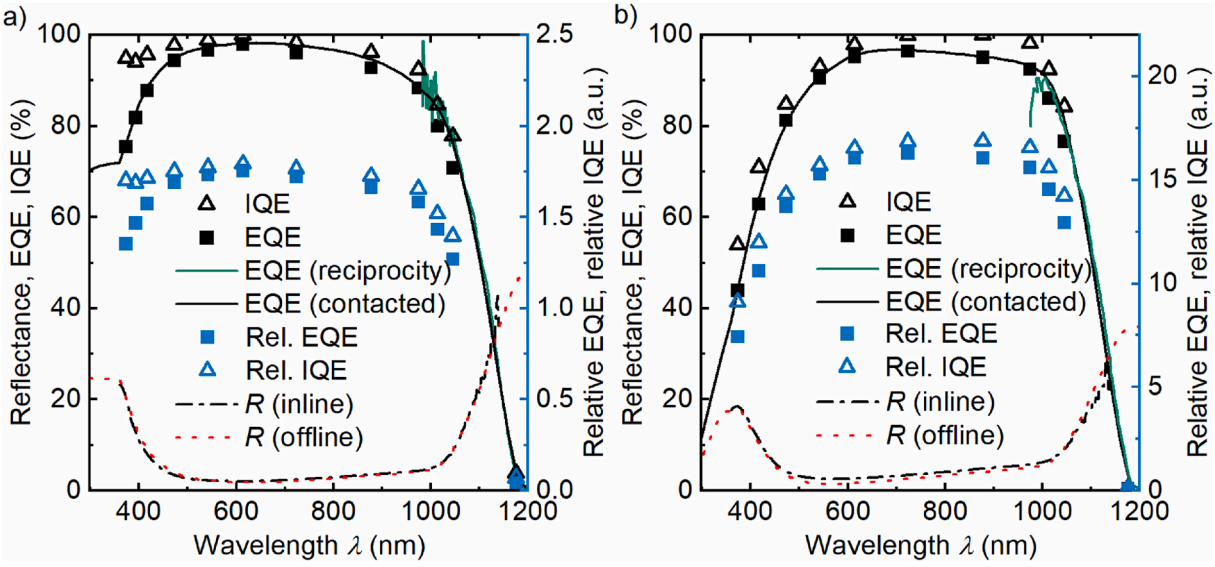

Fig. 2. Reflectance and spectral response data for a) a PERC cell and b) a SHJ cell of the test set illustrate the procedure of scaling the maximum of the relative IQE to 100%, and show that the different EQE data (contactless with ELE (symbols), from luminescence spectrum using the reciprocity theorem (green line), conventional contacted measurement (black line)) agree well with each other. (For interpretation of the references to colour in this figure legend, the reader is referred to the Web version of this article.)

In a continuously running cell production line, this deviation may be decreased or completely avoided by assuming for all cells of the line a correspondingly lower scaling factor S determined on a reference or calibration cell. But this deviation also points to a weakness of the IQE scaling in particular for back-junction solar cells since the precise value of the maximum IQE is not determined contactlessly for each cell individually. More work is required to reduce this deviation further.

4.3. Series resistance

For the series resistance r_s, a clear correlation of the contacted and contactless data can be observed, too, as shown in Fig. 4. We observe an excellent agreement for small r_s, while for larger r_s, the contactless values are up to 23% lower than the equivalent contacted values. The root cause analysis requires further work and will clarify if this is specific for the present cells or applies in general. This analysis will have to take into account the dependence of r_s on the operating conditions (illumination, current, voltage), as discussed, e.g., in Refs. [30,31], both for the contactless and contacted approach. Nevertheless, typical state-of-the-art solar cells will not have such high r_s but will be well below 1 Ωcm^2. Furthermore, the present r_s deviations appear to be large, but their impact on the FF deviation is substantially lower, as shown in Fig. 1b, where we observe a good correlation with mean absolute deviations below 1.3%$_{abs}$.

4.4. Actual IV characteristics and efficiency

The procedure to obtain the actual current-voltage characteristics is illustrated in Fig. 5 for a PERC cell as an example. First, the Suns-PL data is converted to Suns-V_{oc} data via the calibration constant C. Then, the incident light intensity of 1 sun is identified with the j_{sc} at 1 sun illumination as determined from the QE data, and the curve is shifted by - j_{sc} to obtain the $j_{sc}(V_{oc})$ characteristics [32]. Incorporating the voltage drop at the series resistance yields the actual $j(V)$ characteristics. As shown in Fig. 5, a close match with the conventionally measured curves is obtained for the PERC cell.

With this approach, we obtain a good correlation of the contacted and contactless efficiency, as shown in Fig. 6, with a mean absolute deviation of 0.50%$_{abs}$, which corresponds to less than 2.5%$_{rel}$. The analysis of the relative deviations (see Table 1) shows that FF (caused by r_s) and j_{sc} are the most important sources of η deviations here. The deviation of η is in the range of the overall measurement uncertainty specified by certified calibration laboratories (see e.g. Ref. [33]) and may be reduced in the future by streamlining and optimizing the measurement sequence. In a running production, tracking relative changes is often sufficient and the deviations could be reduced by empirically scaling to the conventionally measured quantities. We assume that further work for reducing the deviations is most beneficial if the following parts are addressed: (i) extending the reflectance measurement to the whole sample, (ii) optimizing the scaling of the IQE and (iii)

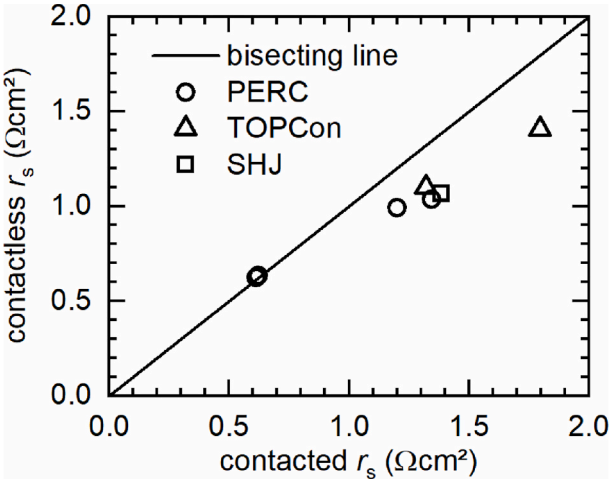

Fig. 4. The comparison of the series resistance r_s of the test set consisting of PERC, TOPCon and SHJ solar cells measured in a contactless and a conventional contacted way show a clear correlation. A systematic underestimation for large r_s can be observed.

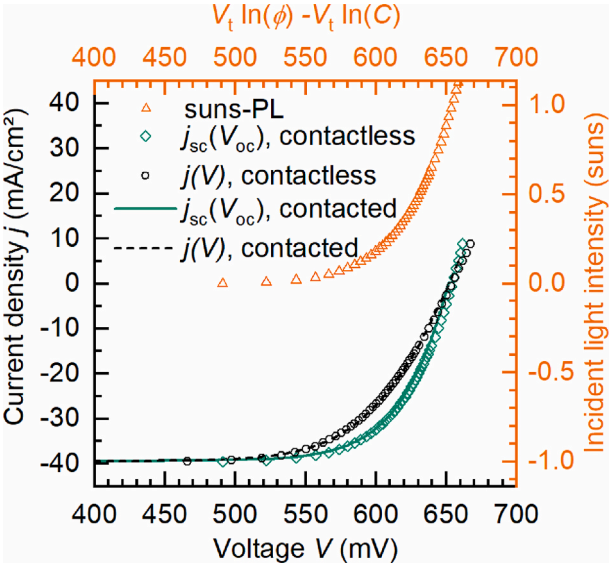

Fig. 5. The Suns-PL data, shown here for a PERC cell, are scaled and shifted based on j_{sc} at 1 sun to obtain the $j_{sc}(V_{oc})$ characteristics. The series resistance r_s induces a voltage drop, converting it into the actual current-voltage. *characteristics.*

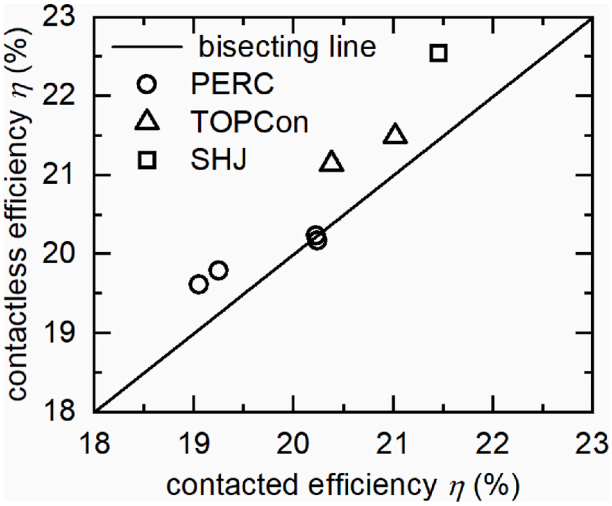

Fig. 6. The comparison of the energy conversion efficiency of the test set consisting of PERC, TOPCon and SHJ solar cells measured in a contactless and a conventional contacted way show a clear correlation.

Table 1
The deviations between contacted and contactless measurements of the most important performance parameters of the test set show j_{sc} and FF as major sources of η deviation.

	V_{oc}	j_{sc}	η	FF	pFF
Mean absolute deviation	2.1 mV	0.32 mA/cm^2	0.50%	1.2%	0.39%
Mean rel. deviation / %$_{rel}$	0.32	0.83	2.5	1.7	0.47

understanding and reducing the observed r_s deviations, where the impact of lateral inhomogeneities of the device under test and the impact of the operating conditions during r_s measurement can be important.

4.5. Measurement speed

As argued above, the measurement speed of the Suns-PL and reflectance measurement lie in the range of 40–50 ms with the metrology used for the present work. For ELE, there is a commercial inline system available [13,34]. For the three PL measurements to determine r_s, we applied PL imaging with a camera with rather long integration times to get sharp and low-noise images but expect similarly short measurement times as for the Suns-PL characteristics or below when using a photodiode as a sensor. We do not expect the integration times but rather transient or hysteresis effects to be ultimately limiting, as is currently the case for conventional inline *IV* measurements [35].

5. Conclusion

We presented an approach do determine the current-voltage (*IV*) characteristics of silicon solar cells under forward bias in a contactless way based on Suns-photoluminescence, spectrophotometry, electroluminescence excitation spectroscopy, and partially shaded photoluminescence. No electrical and mechanical contacting is required, and further information, e.g. the quantum efficiency of the cells is obtained in addition to standard light *IV* parameters. We described the theory and the metrology required for the approach, applied it to a test set of 7 solar cells (PERC, TOPCon, SHJ) and discussed the results including the performance parameters open-circuit voltage V_{oc}, pseudo fill factor pFF, reflectance, quantum efficiency, short-circuit current density j_{sc}, fill factor FF, series resistance, and efficiency η. Good correlations for all these parameters have been observed between contacted reference and contactless measurement data for all investigated cells: The deviations between the contacted and contactless measured current-voltage parameters (j_{sc}, V_{oc}, FF, pFF, η) are below 2.5%$_{rel}$ and, hence, are in the same range as the typical absolute measurement uncertainty of calibrated test laboratories. We conclude that the proof of principle of the contactless determination of current-voltage characteristics is demonstrated successfully. We argued that the measurement speed is ultimately limited by the transient or hysteresis effects, i.e., by the cell physics, not by the metrology.

Reverse current-voltage characteristics may in the future be determined either using sliding or rolling contacts with relaxed requirements on contacting quality or in a contactless way via capacitive or inductive coupling.

CRediT authorship contribution statement

Johannes M. Greulich: Writing – original draft, Methodology, Investigation, Funding acquisition, Formal analysis, Data curation, Conceptualization. **Wiebke Wirtz:** Writing – review & editing, Methodology, Investigation, Formal analysis, Data curation. **Hannes Höffler:** Writing – review & editing, Validation, Supervision, Methodology, Conceptualization. **Nico Wöhrle:** Methodology, Funding acquisition, Conceptualization. **Mattias K. Juhl:** Writing – review & editing, Validation, Supervision, Methodology. **Oliver Kunz:** Writing – review & editing, Validation, Investigation, Formal analysis, Data curation. **Stefan Rein:** Writing – review & editing, Validation, Supervision, Funding acquisition. **Andreas W. Bett:** Writing – review & editing, Supervision.

Declaration of competing interest

The authors declare the following financial interests/personal relationships which may be considered as potential competing interests:

Johannes Greulich has patent pending to Fraunhofer-Gesellschaft zur Förderung der angewandten Forschung e.V.

Data availability

Data will be made available on request.

Acknowledgements

This work was financially supported by the German Federal Ministry for Economic Affairs and Climate Action and by industry partners within the research project “NextTec” under grant number 03EE1001A. We thank Felix Martin and Appu Paduthol for assistance with ELE measurements at Fraunhofer ISE and UNSW.

References

[1] M. Alt, S. Fischer, S. Schenk, S. Zimmermann, K. Ramspeck, M. Meixner, Electroluminescence imaging and automatic cell classification in mass production of silicon solar cells, in: 7th World Conference on Photovoltaic Energy Conversion (WCPEC), Waikoloa, Hawaii, USA, 2018, pp. 3298–3304, https://doi.org/10.1109/PVSC.2018.8547983.

[2] D.L. King, J.M. Gee, B.R. Hansen, Measurement precautions for high-resistivity silicon solar cells, in: Conference Record of the Twentieth IEEE Photovoltaic Specialists Conference, Las Vegas, NV, USA, IEEE, 9/26/1996 - 9/30/1988, 555-559. https://doi.org/10.1109/PVSC.1988.105763.

[3] R.A. Sinton, H.W. Wilterdink, A.L. Blum, Assessing transient measurement errors for high-efficiency silicon solar cells and modules, IEEE J. Photovoltaics 7 (2017) 1591–1595, https://doi.org/10.1109/JPHOTOV.2017.2753200.

[4] P. Baliozian, N. Klasen, N. Wöhrle, C. Kutter, H. Stolzenburg, A. Münzer, P. Saint-Cast, M. Mittag, E. Lohmüller, T. Fellmeth, M. Al-Akash, A. Kraft, M. Heinrich, A. Richter, A. Fell, A. Spribille, H. Neuhaus, R. Preu, PERC-based shingled solar cells and modules at Fraunhofer ISE, Photovolt. Int. (2019) 129–145.

[5] T. Trupke, R.A. Bardos, M.D. Abbott, J.E. Cotter, Suns-photoluminescence: contactless determination of current-voltage characteristics of silicon wafers, Appl. Phys. Lett. 87 (2005), 93503, https://doi.org/10.1063/1.2034109.

[6] A. Krieg, J. Greulich, M. Tondorf, S. Rein, Anti-reflection-coating thickness measurements on textured silicon surfaces: evaluation and accuracy of different measurement techniques, in: 28th European Photovoltaic Solar Energy Conference and Exhibition, France, Paris, 2013, pp. 1820–1824, https://doi.org/10.4229/28thEUPVSEC2013-2CV.4.56.

[7] R.A. Sinton, Contactless electroluminescence for shunt-value measurement in solar cells, in: 23rd European Photovoltaic Solar Energy Conference and Exhibition, Proceedings, Valencia, Spain, 2008, pp. 1157–1159, https://doi.org/10.4229/23rdEUPVSEC2008-2DO.2.1.

[8] M.D. Abbott, R.A. Bardos, T. Trupke, K.C. Fisher, E. Pink, The effect of diffusion-limited lifetime on implied current voltage curves based on photoluminescence data, J. Appl. Phys. 102 (2007), 44502, https://doi.org/10.1063/1.2756529.

[9] H. Mäckel, A. Cuevas, Spectral response of the photoconductance: a new technique for solar cell characterization, in: International Solar Energy Society World Congress, Adelaide, Australia, Australian and New Zealand Solar Energy Society, Adelaide, 2001.

[10] D. Berdebes, J. Bhosale, K.H. Montgomery, X. Wang, A.K. Ramdas, J.M. Woodall, M.S. Lundstrom, Photoluminescence excitation spectroscopy for in-line optical characterization of crystalline solar cells, IEEE J. Photovoltaics 3 (2013) 1342–1347, https://doi.org/10.1109/JPHOTOV.2013.2278884.

[11] M.K. Juhl, M.D. Abbott, T. Trupke, Relative external quantum efficiency of crystalline silicon wafers from photoluminescence, IEEE J. Photovoltaics 7 (2017) 1074–1080, https://doi.org/10.1109/JPHOTOV.2017.2697313.

[12] M.K. Juhl, T. Trupke, The impact of voltage independent carriers on implied voltage measurements on silicon devices, J. Appl. Phys. 120 (2016), 165702, https://doi.org/10.1063/1.4965698.

[13] K.O. Davis, G.S. Horner, J.B. Gallon, L.A. Vasilyev, K.B. Lu, A.B. Dirriwachter, T. B. Rigdon, E.J. Schneller, K. Öğütman, R.K. Ahrenkiel, Electroluminescence excitation spectroscopy: a novel approach to non-contact quantum efficiency measurements, in: 44th IEEE Photovoltaic Specialists Conference, PVSC), Washington, DC, USA, 2017, pp. 3448–3451, https://doi.org/10.1109/PVSC.2017.8366170.

[14] A. Paduthol, M.K. Juhl, T. Trupke, Addressing limitations of photoluminescence based external quantum efficiency measurements, J. Appl. Phys. 123 (2018), 23105, https://doi.org/10.1063/1.5004193.

[15] A. Paduthol, M.K. Juhl, T. Trupke, Correcting the effect of LED spectra on external quantum efficiency measurements of solar cells, IEEE J. Photovoltaics 8 (2018) 559–564, https://doi.org/10.1109/JPHOTOV.2017.2787022.

[16] U. Rau, Reciprocity relation between photovoltaic quantum efficiency and electroluminescent emission of solar cells, Phys. Rev. B 76 (2007) 1–8, https://doi.org/10.1103/PhysRevB.76.085303.

[17] T. Kirchartz, A. Helbig, W. Reetz, M. Reuter, J.H. Werner, U. Rau, Reciprocity between electroluminescence and quantum efficiency used for the characterization of silicon solar cells, Prog. Photovoltaics Res. Appl. 17 (2009) 394–402, https://doi.org/10.1002/pip.895.

[18] M. Kasemann, L.M. Reindl, B. Michl, W. Warta, A. Schütt, J. Carstensen, Contactless qualitative series resistance imaging on solar cells, IEEE J. Photovoltaics 2 (2012) 181–183, https://doi.org/10.1109/jphotov.2012.2184524.
[19] Y. Zhu, M.K. Juhl, T. Trupke, Z. Hameiri, Photoluminescence imaging of silicon wafers and solar cells with spatially inhomogeneous illumination, IEEE J. Photovoltaics 7 (2017) 1087–1091, https://doi.org/10.1109/JPHOTOV.2017.2690875.
[20] I. Zafirovska, M.K. Juhl, J.W. Weber, J. Wong, T. Trupke, Detection of finger interruptions in silicon solar cells using line scan photoluminescence imaging, IEEE J. Photovoltaics 7 (2017) 1496–1502, https://doi.org/10.1109/JPHOTOV.2017.2732220.
[21] H. Höffler, W. Wirtz, J.M. Greulich, S. Rein, Quantitative contactless determination of the series resistance of silicon solar cells, in: 38th European Photovoltaic Solar Energy Conference and Exhibition, 2021, pp. 233–236, https://doi.org/10.4229/EUPVSEC20212021-2CV.1.5. Online.
[22] A. Paduthol, Contactless Spectral Response Measurement of Solar Cells Using Photoluminescence, PhD thesis, 2019, p. 64.
[23] M. Juhl, Application of the Spectral Response of Photoluminescence in Photovoltaics, PhD thesis, 2017, p. 94.
[24] B. Fischer, J. Müller, P.P. Altermatt, A simple emitter model for quantum efficiency curves and extracting the emitter saturation current, in: 28th European Photovoltaic Solar Energy Conference and Exhibition, France, Paris, 2013, pp. 840–845, https://doi.org/10.4229/28thEUPVSEC2013-2BO.3.4.
[25] P.A. Basore, Extended spectral analysis of internal quantum efficiency, in: 23rd IEEE Photovoltaic Specialists Conference (PVSC). Conference Record, Louisville, KY, USA, 1993, pp. 147–152, https://doi.org/10.1109/pvsc.1993.347063.
[26] T. Tiedje, E. Yablonovitch, G.D. Cody, B.G. Brooks, Limiting efficiency of silicon solar cells, IEEE Trans. Electron. Dev. 31 (1984) 711–716, https://doi.org/10.1109/t-ed.1984.21594.
[27] N. Bassi, C. Clerc, Y. Pelet, J. Hiller, V. Fakhfouri, C. Droz, M. Despeisse, J. Levrat, A. Faes, D. Bätzner, P. Papet, GridTOUCH: innovative solution for accurate IV measurement of busbarless cells in production and laboratory environments, in: 29th European Photovoltaic Solar Energy Conference and Exhibition, Amsterdam, The Netherlands, 2014, https://doi.org/10.4229/EUPVSEC20142014-2BV.8.24.
[28] H. Höffler, F. Schindler, A. Brand, D. Herrmann, R. Eberle, R. Post, A. Kessel, J. Greulich, M.C. Schubert, Review and recent development in combining photoluminescence- and electroluminescence-imaging with carrier lifetime measurements via modulated photoluminescence at variable temperatures, in: 37th European Photovoltaic Solar Energy Conference and Exhibition, 2020, pp. 264–276, https://doi.org/10.4229/EUPVSEC20202020-2CO.14.2. Online.
[29] M. Hermle, F. Granek, O. Schultz, S.W. Glunz, Analyzing the effects of front-surface fields on back-junction silicon solar cells using the charge-collection probability and the reciprocity theorem, J. Appl. Phys. 103 (2008), 54507, https://doi.org/10.1063/1.2887991.
[30] K.C. Fong, K.R. McIntosh, A.W. Blakers, Accurate series resistance measurement of solar cells, Prog. Photovoltaics Res. Appl. 21 (2013) 490–499, https://doi.org/10.1002/pip.1216.
[31] J.-M. Wagner, K. Upadhyayula, J. Carstensen, R. Adelung, A critical review and discussion of different methods to determine the series resistance of solar cells: $R_{s,dark}$ vs $R_{s,light}$? AIP Conf. Proc. 1999 (2018), 020022 https://doi.org/10.1063/1.5049261.
[32] R.A. Sinton, A. Cuevas, A quasi-steady-state open-circuit voltage method for solar cell characterization, in: 16th European Photovoltaic Solar Energy Conference, Proceedings, Glasgow, UK, 2000, pp. 1152–1155.
[33] M.A. Green, E.D. Dunlop, J. Hohl-Ebinger, M. Yoshita, N. Kopidakis, X. Hao, Solar cell efficiency tables (Version 58), Prog. Photovoltaics Res. Appl. 29 (2021) 657–667, https://doi.org/10.1002/pip.3444.
[34] Tau Science Corporation, Electroluminescence excitation spectroscopy of semiconductors: a tau science technical whitepaper. http://tauscience.com/ele. (Accessed 20 April 2022).
[35] K. Ramspeck, S. Schenk, L. Komp, A. Metz, M. Meixner, Accurate efficiency measurements on very high efficiency silicon solar cells using pulsed light sources, in: 29th European Photovoltaic Solar Energy Conference and Exhibition, The Netherlands, Amsterdam, 2014, pp. 1253–1256, https://doi.org/10.4229/EUPVSEC20142014-2BV.8.49.